ZnO nanorods for efficient third harmonic UV generation

Susanta Kumar Das,[1,4] Frank Güell,[2] Ciarán Gray,[3] Prasanta Kumar Das[4], Ruediger Grunwald,[1] and Enda McGlynn[3,*]

[1]*Max-Born-Institut für Nichtlineare Optik und Kurzzeitspektroskopie, Max-Born-Strasse 2a, D-12489 Berlin, Germany*
[2]*Departament d'Electrònica, Universitat de Barcelona, C/Martí i Franquès 1, E-08028 Barcelona, Catalunya, Spain*
[3]*School of Physical Sciences, National Centre for Plasma Science and Technology, Dublin City University, Glasnevin, Dublin 9, Ireland*
[4]*School of Applied Sciences, KIIT University, Bhubaneswar - 751024, Odisha, India*
[*]*enda.mcglynn@dcu.ie*

Abstract: ZnO nanorods grown by both high temperature vapour phase transport and low temperature chemical bath deposition are very promising sources for UV third harmonic generation. Material grown by both methods show comparable efficiencies, in both cases an order of magnitude higher than surface third harmonic generation at the quartz-air interface of a bare quartz substrate. This result is in stark contrast to the linear optical properties of ZnO nanorods grown by these two methods, which show vastly different PL efficiencies. The third harmonic generated signal is analysed using intensity dependent measurements and interferometric frequency resolved optical gating, allowing extraction of the laser pulse parameters. The comparable levels of efficiency of ZnO grown by these very different methods as sources for third harmonic UV generation provides a broad suite of possible growth methods to suit various substrates, coverage and scalability requirements. Potential application areas range from interferometric frequency resolved optical gating characterization of few cycle fs pulses to single cell UV irradiation for biophysical studies.

©2014 Optical Society of America

OCIS codes: (160.4236) Nanomaterials; (190.4400) Nonlinear optics, materials; (190.7110) Ultrafast nonlinear optics.

References and links

1. A. B. Djurisić and Y. H. Leung, "Optical properties of ZnO nanostructures," Small **2**(8-9), 944–961 (2006).
2. D. Byrne, E. McGlynn, J. Cullen, and M. O. Henry, "A catalyst-free and facile route to periodically ordered and c-axis aligned ZnO nanorod arrays on diverse substrates," Nanoscale **3**(4), 1675–1682 (2011).
3. E. McGlynn, M. O. Henry, and J.-P. Mosnier, "ZnO wide bandgap semiconductor nanostructures: growth, characterisation and applications," in *Handbook of Nanoscience and Technology vol. II*, A.V. Narlikar and Y.Y.Fu, eds. (Oxford University Press, 2009).
4. G. I. Petrov, V. Shcheslavskiy, V. V. Yakovlev, I. Ozerov, E. Chelnokov, and W. Marine, "Efficient third-harmonic generation in a thin nanocrystalline film of ZnO," Appl. Phys. Lett. **83**(19), 3993–3995 (2003).
5. K. Wang, J. Zhou, L. Y. Yuan, Y. T. Tao, J. Chen, P. X. Lu, and Z. L. Wang, "Anisotropic third-order optical nonlinearity of a single ZnO micro/nanowire," Nano Lett. **12**(2), 833–838 (2012).
6. S. K. Das, M. Bock, C. O'Neil, R. Grunwald, K. Lee, H. Lee, S. Lee, and F. Rotermund, "Efficient second harmonic generation in ZnO nanorod arrays with broadband ultrashort pulses," Appl. Phys. Lett. **93**(18), 181112 (2008).
7. K. Pedersen, C. Fisker, and T. G. Pedersen, "Second-harmonic generation from ZnO nanowires," Phys. Status Solidi **5**(8 c), 2671–2674 (2008).
8. Y. Kobayashi, D. Yoshitomi, K. Iwata, H. Takada, and K. Torizuka, "Ultrashort pulse characterization by ultra-thin ZnO, GaN, and AlN crystals," Opt. Express **15**(15), 9748–9754 (2007).
9. S. K. Das, C. Schwanke, A. Pfuch, W. Seeber, M. Bock, G. Steinmeyer, T. Elsaesser, and R. Grunwald, "Highly efficient THG in TiO2 nanolayers for third-order pulse characterization," Opt. Express **19**(18), 16985–16995 (2011).
10. C. Zhang, F. Zhang, S. Qian, N. Kumar, J. Hahm, and J. Xu, "Multi-photon absorption induced amplified spontaneous emission from biocatalyst synthesized ZnO nanorods," Appl. Phys. Lett. **92**(23), 233116 (2008).
11. D. Sridhar, X. Jining, J. K. Abraham, and V. K. Varadan, "Synthesis and photonic property study of ZnO nanowires for a real time photodynamic therapy monitoring probe," Proc. SPIE **6528**, 65281L (2007).

12. C. Baratto, E. Comini, G. Faglia, G. Sberveglieri, M. Zha, and A. Zappettini, "Metal oxide nanocrystals for gas sensing," Sens. Actuators B Chem. **109**(1), 2–6 (2005).
13. J. Li, D. Guo, X. Wang, H. Wang, H. Jiang, and B. Chen, "The photodynamic effect of different size ZnO nanoparticles on cancer cell proliferation in vitro," Nanoscale Res. Lett. **5**(6), 1063–1071 (2010).
14. S. M. Al-Hilli, M. Willander, A. Öst, and P. Strålfors, "ZnO nanorods as an intracellular sensor for pH measurements," J. Appl. Phys. **102**(8), 084304 (2007).
15. D. Byrne, E. McGlynn, M. Biswas, M. O. Henry, K. Kumar, and G. Hughes, "A Study of drop-coated and chemical bath-deposited buffer layers for vapor phase deposition of large area, aligned, zinc oxide nanorod arrays," Cryst. Growth Des. **10**(5), 2400–2408 (2010).
16. D. Byrne, E. McGlynn, M. O. Henry, K. Kumar, and G. Hughes, "A novel, substrate independent three-step process for the growth of uniform ZnO nanorod arrays," Thin Solid Films **518**(16), 4489–4492 (2010).
17. F. Güell, J. O. Osso, A. R. Goni, A. Cornet, and J. R. Morante, "Synthesis and optical spectroscopy of ZnO nanowires," Superlattices Microstruct. **45**(4-5), 271–276 (2009).
18. F. Güell, J. O. Ossó, A. R. Goñi, A. Cornet, and J. R. Morante, "Direct imaging of the visible emission bands from individual ZnO nanowires by near-field optical spectroscopy," Nanotechnology **20**(31), 315701 (2009).
19. T. Y. F. Tsang, "Optical third-harmonic generation at interfaces," Phys. Rev. A **52**(5), 4116–4125 (1995).
20. U. Neumann, R. Grunwald, U. Griebner, G. Steinmeyer, M. Schmidbauer, and W. Seeber, "Second harmonic performance of a-axis oriented ZnO nanolayers on sapphire substrates," Appl. Phys. Lett. **87**(17), 171108 (2005).
21. G. Stibenz and G. Steinmeyer, "Interferometric frequency-resolved optical gating," Opt. Express **13**(7), 2617–2626 (2005).
22. G. Stibenz and G. Steinmeyer, "Structures of interferometric frequency-resolved optical gating," IEEE J. Sel. Top. Quantum Electron. **12**(2), 286–296 (2006).
23. A. Anderson, K. S. Deryckx, X. G. Xu, G. Steinmeyer, and M. B. Raschke, "Few-femtosecond plasmon dephasing of a single metallic nanostructure from optical response function reconstruction by interferometric frequency resolved optical gating," Nano Lett. **10**(7), 2519–2524 (2010).
24. http://www.rp-photonics.com/chromatic_dispersion.html.

1. Introduction

ZnO nanostructures offer an exceptionally interesting and broad range of nanomorphologies and growth methods, with various advantages and disadvantages in terms of potential applications [1]. For example, ZnO can be grown by higher temperature techniques such as vapour phase transport (VPT) and by lower temperature techniques such as chemical bath deposition (CBD), the former yielding deposited material with excellent optical emission properties, but generally over limited substrate sizes and the latter being particularly amenable to uniform, large area, depositions where scaleability is required, but yielding material with characteristically poor optical properties such as photoluminescence emission [2, 3]. Thus trade-offs in terms of linear optical properties and scaleability are inherent in the different growth methods of ZnO nanostructures. The nonlinear optical properties of such materials, especially the third order nonlinearities and their variation between materials grown by different methods, are much less studied. Third harmonic generation (THG) has been reported from ZnO nanomaterials [4, 5], and quite a few publications deal with second harmonic generation (SHG) from this material and its nanostructures [6, 7].

Further studies of frequency conversion are important because UV light generation via efficient THG in ZnO nanostructures offers many possible applications. One example is the characterization of ultrashort, few cycle fs laser pulses. Characterization of such pulses is rendered complex by the ultrashort, broadband, nature of such pulses (> 100 nm) where dispersive effects can be dominant and thus one needs extremely thin nonlinear crystals for faithful pulse characterization [8]. Recently our group has demonstrated the use of TiO_2 nanocrystalline thin films to characterize pulses as short as 20 fs, demonstrating the utility of nanostructured metal oxides for such applications, where the nano length scales allow one to avoid phase-matching constraints associated with traditional bulk nonlinear materials [9].

Furthermore, the efficient generation of UV light within the human body, either by coupling NIR radiation through the "tissue optical window" wavelength range 0.7–1.1 μm or via optical waveguides into nanowires or nanorods embedded in body tissue, may enable new methods of local UV photodynamic therapy, even to the level of single cell studies, if suitably high conversion efficiencies into the UV spectral range can be realised [10–14]. In regard to the case of single cell studies, it is noteworthy that previous measurements of quantities within a single cell have successfully utilised ZnO nanorods deposited by CBD on a borosilicate glass capillary [14].

In this work we report studies of THG by ZnO nanorod samples grown by both VPT and CBD. We show that the THG efficiency of both types of samples is comparable, and significantly higher than that observed at the surface of a bare quartz sample. We characterize the THG generated by both sample types using both intensity dependence and interferometric frequency resolved optical gating (iFROG) measurements, and extract the laser pulse parameters for situations of both high and low pulse chirp. We conclude that ZnO nanomaterials of these types yield faithful pulse characterization for pulses of original widths < 10 fs and efficient THG, and thus are excellent prospects for the application areas mentioned above.

2. Experimental details

Experimental details on growth and characterization of ZnO nanostructures

ZnO nanostructures were grown by both CBD (on fused silica substrates) and by VPT (on (11-20) sapphire substrates). The details of the growth method used for CBD have been given elsewhere [3, 15, 16]. In summary, fused silica substrates (Alfa Aeser, product code 42295), were cleaned by sonication in acetone followed by ethanol and dried in a nitrogen stream. They were then coated with a ZnO seed layer by drop coating a 5 mM solution of zinc acetate in absolute ethanol. 3.75 μl of zinc acetate solution per cm^2 of substrate was applied to the substrate surface for 20 seconds before being rinsed with absolute ethanol and dried with a nitrogen stream. This drop coating procedure was repeated a further four times and following this the samples were annealed at 350°C in air for 30 min. ZnO nanorods were then deposited on the acetate-derived seed layer. A solution of 0.02 M zinc nitrate was slowly added to an equal volume of 0.8 M NaOH solution while stirring vigorously. This solution was heated to 70°C before the substrates were submerged in the mixture. This temperature was maintained for 25 min, with gentle stirring. After this time, the substrates were removed from the reaction solution, washed with DI-H_2O, and dried with nitrogen. As the results in the next section demonstrate, the samples grown by this method form a film of densely packed ZnO nanorods, with a thickness of ~1 μm and an average nanorod diameter of ~75 nm. The nanorods are highly textured perpendicular to the substrate surface by virtue of the acetate seeding stage.

The details of the growth method used for VPT are as follows (more detail may be found in references 17 and 18) [17, 18]. An Au catalyzed vapour-liquid-solid (VLS) process was used to grow the ZnO nanorods on sapphire substrates. We have used three substrates with different crystallographic directions: c-plane (0001), a-plane (11-20) and r-plane (1-102), although the results shown below are for samples grown on a-plane (11-20) substrates which had a dense coverage of well-aligned nanorods with an average length of ~0.6 μm and an average nanorod diameter of ~70 nm. The catalyst was deposited on the substrates by sputtering, forming a 3 nm thick gold layer. ZnO powder was mixed with graphite powder and the synthesis was carried out in a horizontal quartz tube placed in a CVD furnace. Ar was used as an inert gas and the furnace was heated at 900°C for 30 min.

The similarity of nanorod morphology and dimensions for the samples grown by both CBD and VPT allows a meaningful comparison of their nonlinear optical behaviours without effects due to differing morphologies affecting our conclusions.

The samples were characterized after deposition by field emission SEM (FESEM; JEOL JSM-6400F and Hitachi H-4100FE) and x-ray diffraction (XRD; Bruker AXS D8 Advance Texture Diffractometer).

Experimental details on third harmonic generation with ultrashort pulses

THG experiments were carried out using a Ti:sapphire laser from Venteon Femtosecond Laser Technologies, pumped by a frequency doubled Nd:YAG laser. The temporal width, repetition rate and energy of the pulses exiting the laser were ~7 fs, 80 MHz and ~5.25 nJ, respectively. The central wavelength of the laser is ~810 nm and the bandwidth full width at half maximum (FWHM) is > 300 nm. The laser was focussed onto the sample with a beam waist of ~4 μm, yielding a peak intensity of ~1.5 x 10^{12} W/cm^2 in the un-attenuated direct

beam. iFROG measurements were taken using a home-built system, based on a Michelson interferometer with one mirror driven by a piezoelectric motion controller with a step size of 35 nm. The delayed and re-combined pulses are incident on the samples under the conditions described above and the THG signal is separated from residual pump radiation by a THG reflecting mirror and an interference filter and analyzed with a fibre-coupled high sensitivity electron multiplier charge coupled device (EMCCD)-based spectrometer (Newton, Andor Technology). All experiments were carried out at room temperature and the EMCCD was internally cooled down to −75 °C electronically. The motion of the interferometer mirror and the spectrometer spectrum capture were synchronized by using an in-house developed LabView programme. Subsequent analysis of the iFROG data was done using commercial Femtosoft software (Femtosoft Technologies, FROG 3.0) after Fourier filtering to extract ordinary FROG data.

3. Results and discussion

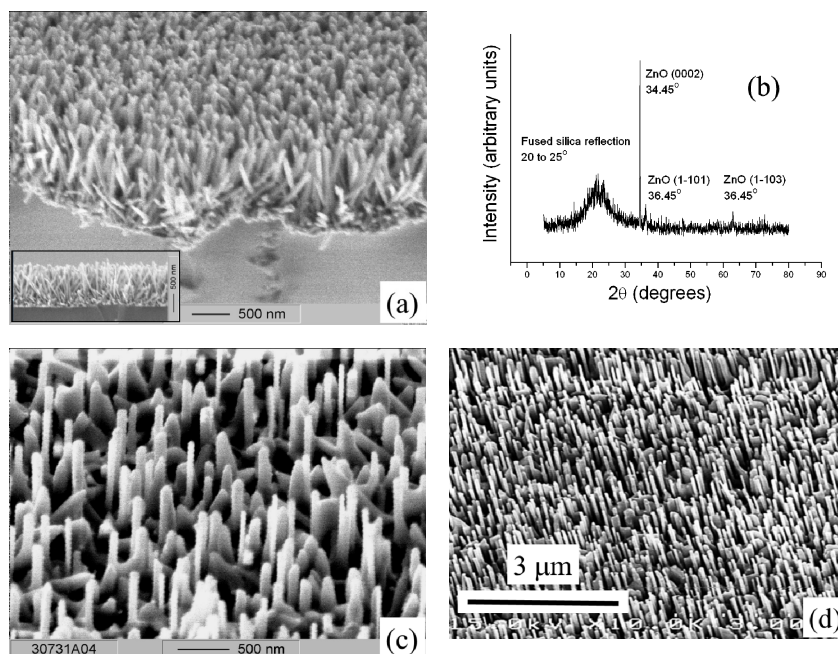*Structural properties and fs-laser induced UV-spectra of ZnO-nanorods*

Fig. 1. (a) FESEM data (45° tilted-view image) of the CBD grown ZnO nanorod sample (inset, cross-sectional view); (b) θ-2θ XRD data from the same sample; (c) and (d) show FESEM data for the VPT-grown ZnO nanorod sample grown on sapphire.

Figure 1(a) contains FESEM data of the CBD grown ZnO nanorod sample showing a film of densely packed ZnO nanorods, with a thickness of ~1 μm (inset, cross-sectional view) with an average nanorod diameter of ~75 nm (main, 45° tilted-view image). The nanorods show good texture normal to the substrate. Figure 1(b) contains θ-2θ XRD data from the same sample, and the dominant XRD reflection at ~34.45° is associated with the ZnO (0002) reflection, this texture confirming the good alignment of the nanorods also seen in the SEM data. The broad reflection in the region 20° to 25° is associated with the fused silica substrate. Figures 1(c) and 1(d) show FESEM data for the VPT grown ZnO nanorod sample grown on sapphire. XRD data from VPT grown samples on (11-20) sapphire substrates (data not shown) show a similar diffraction pattern to that seen for the CBD grown sample, with a dominant ZnO

(0002) reflection due to the highly textured, well-aligned nanorod morphology seen in the SEM data in Figs. 1(c) and 1(d).
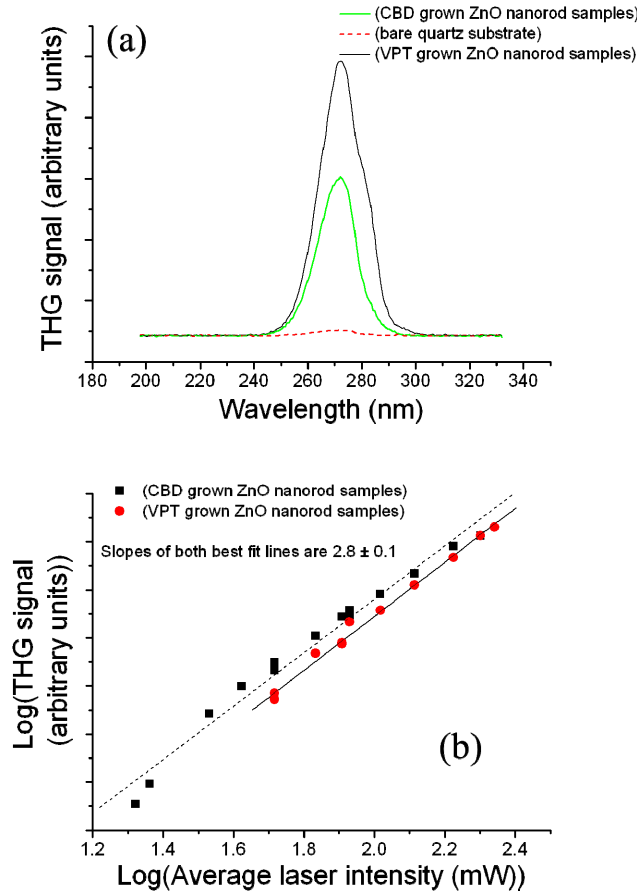

Fig. 2. (a) THG spectra in the region 197 nm to 332 nm for both the CBD and VPT grown ZnO nanorod samples as well as a bare quartz substrate, under focused illumination by the Ti:sapphire laser; (b) intensity dependence data for both the CBD and VPT grown ZnO nanorod samples.

Figure 2(a) shows the THG spectra for both the CBD and VPT grown ZnO nanorod samples under focused illumination by Ti:sapphire laser, with conditions as described earlier (specifically after the beam splitter in the iFROG set-up with fixed and unequal path lengths, leading to a pulse width of ~11 fs). Figure 2(a) also shows the surface enhanced THG (STHG) signal from a bare quartz substrate for comparison, recorded under identical conditions. A spectral signature at ~272 nm with bandwidth of ~20 nm is seen from all samples and this is consistent with THG, either from the ZnO nanrorod deposits or surface THG (STHG) at the quartz-air interface for the case of the bare quartz substrate [19]. This identification with THG for the case of the signal from the ZnO samples is further confirmed by the intensity dependence data shown in Fig. 2(b). For these measurements the laser beam intensity was controlled using combinations of neutral density (ND) filters. The ND filters create additional temporal broadening of the laser pulse to ~42 fs (in addition to chirp effects), leading to a corresponding reduction in the peak intensity during the pulse. However the broadening is not dependent on the specific filters used and the same laser pulse width was measured for a range of filters, examples of which are shown below for different filtering conditions. The

THG signal from both the CBD and VPT grown ZnO nanorod samples is very similar, although the VPT grown sample shows a small shoulder at longer wavelengths, also seen in iFROG data in Fig. 3 below. This shoulder is most probably due to effects of different alignment and/or faceting of the ZnO nanostructures grown by CBD and VPT, since nonlinear processes in such nanostructures often show differences due to the specific crystal termination [20].

The (baseline-corrected) integrated intensity of the signal around 272 nm is plotted versus laser intensity on a log-log graph and the slope of this graph yields the order of the nonlinear process. For the case of THG from the CBD grown ZnO sample the slope is 2.8 ± 0.1, while the value for the VPT grown sample is also 2.8 ± 0.1, both very close to the expected value of 3 for a third order process. The small difference in the experimental values from an exponent of 3 in both cases is most probably due to the departure of the pulse from an ideal "flat-top" temporal profile, which will reduce the measured slope values slightly.

The THG efficiency of both types of ZnO nanorod samples is comparable, and significantly greater than that observed due to STHG at the surface of a bare quartz sample which is at least one order of magnitude less than that from the ZnO nanorod samples. This result contrasts greatly with measurements of the linear optical properties of ZnO nanorods grown by these two methods, which show vastly different PL efficiencies. PL emission from CBD grown ZnO nanorods is always much weaker (and at low temperatures is far more spectrally broad, with individual exciton features unresolved) than that from VPT grown ZnO nanorods [2, 3].

ZnO nanorods as frequency converters for third order pulse characterization with iFROG

Figure 3 shows iFROG data from the CBD and VPT grown ZnO nanorod samples, respectively. The data from both the CBD and VPT grown ZnO nanorod samples are very similar, with the exception of the longer wavelength shoulder seen in the case of the VPT grown sample, mentioned above. Figures 3(a) and 3(d) show the raw third-order iFROG trace for the CBD and VPT grown samples, respectively. By Fourier analysing the iFROG data one can obtain the different order frequency components. The first two order components (i.e. DC and first order) can be analysed to retrieve the pulse shape by two independent methods. Because of the availability of these two methods, iFROG offers an added internal consistency check, in particular for calibrating the delay axis [21–23]. Here we restrict ourselves to analyzing the DC part of the trace that we extract by Fourier filtering. The resulting traces are shown in Figs. 3(b) and 3(e) for the case of the CBD and VPT grown ZnO nanorod samples, respectively. It has been proved that this trace is equivalent to an ordinary frequency resolved optical gating (FROG) trace and hence can be directly be processed by a standard pulse retrieval software. For the present case the resulting FROG trace was processed by commercial software (Femtosoft Technologies, FROG 3.0).The retrieved spectral signal and spectral phase are shown in Figs. 3(c) and 3(f). The corresponding pulse duration is estimated to be ~11 fs in both cases.
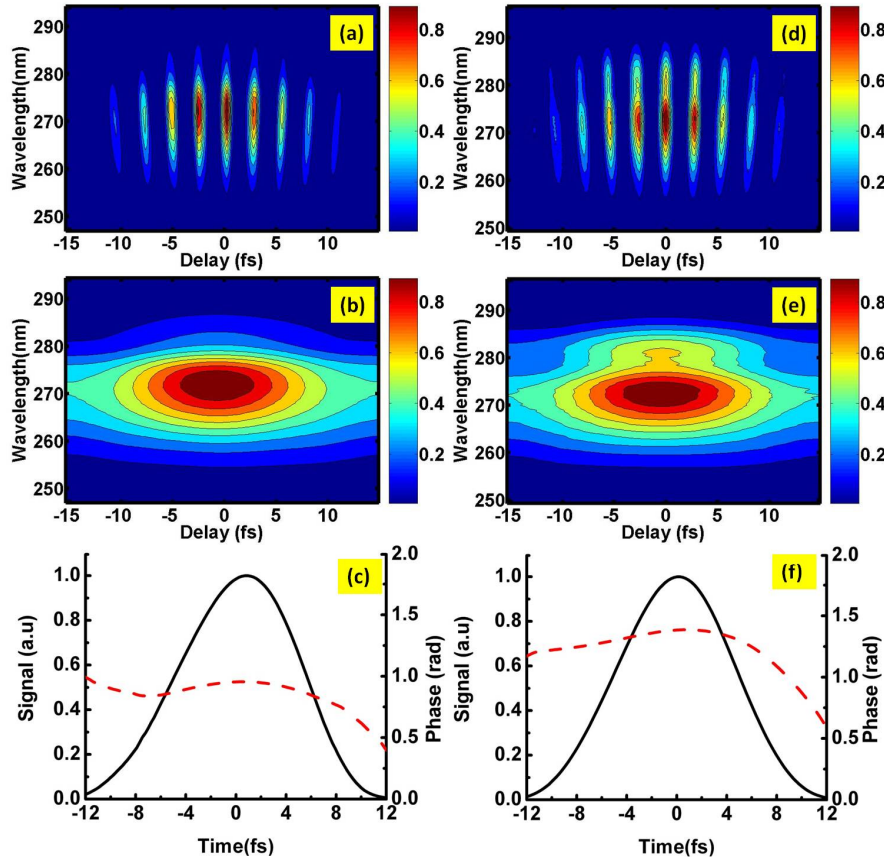
Fig. 3. (a) iFROG trace, (b) FROG and (c) temporal pulse profile measured on ZnO nanorods grown by CBD method; (d) iFROG trace, (e) FROG and (f) temporal pulse profile measured on ZnO nanorods grown by VPT method (in all cases data are taken without any ND filter in the path).

We detail further analysis and results for the CBD grown nanorod sample only since the data for the VPT grown nanorod sample are essentially identical. In this case the time-bandwidth product extracted from the FROG analysis was 0.55. Generally an unchirped pulse of Gaussian profile has a time-bandwidth product of 0.44. The higher time band width found here indicates the presence of quadratic chirp in our pulse. The curved phase profile in Fig. 3(c) clearly indicates the presence of this chirp which we attribute mainly to the beam splitter we used in our iFROG set up. The substrate of this beam splitter was quartz and its thickness was 0.7 mm (Venteon). Generally the group delay dispersion (GDD) of glass is ~36 fs^2/mm [24]. So the net GDD (β_2) introduced by our beam splitter was 24 fs^2 (= 36 fs^2 x 0.7). In presence of GDD, the pulse duration (τ) dependence on GDD is given by Eq. (1) below:

$$\tau = \tau_0 \sqrt{1 + \left(4\ln\left(\frac{\beta_2}{\tau_0^2} \right) \right)^2} \tag{1}$$

where τ_0 = duration of the unchirped pulse coming from the laser [24]. Inserting values for τ (11 fs) and β_2 (24 fs^2) in Eq. (1) the duration of the unchirped pulse was found to be τ_0 = 7 fs, close to the value of 6.7 fs independently measured by a commercial Few Cycle-Spectral Phase Interferometry for Direct Electric-field Reconstruction (FC-SPIDER; Applied Physics and Electronics – APE Ltd., Berlin, Germany) system. This clearly demonstrates the ability of ZnO nanorod samples such as these to successfully measure pulse durations below 10 fs.

Further testing of the pulse diagnostics ability of the ZnO nanorod samples was performed by estimating the pulse parameters of the ultrashort pulses after passing through highly dispersive (HD) media. The metal coated ND filters (New Focus, 2 filter wheel system) which were previously used for intensity variation studies (see Fig. 2) served as a HD medium. We tested the pulse for three sets of filter conditions with significantly different degrees of transmission (specifically corresponding to ND values of 0.04 + 0.04, 0.04 + 0.2, 0.04 + 0.4; the two numbers referring to the ND optical density of the two filters in the combination). The typical iFROG and FROG (DC component of iFROG) traces and the pulse shapes of the ultrashort pules after passing through the ND filter are shown in Figs. 4(a)-4(i), using the CBD grown nanorod sample. FROG analysis shows the duration of the pulse for each filter condition to be constant at ~42 fs. This much longer duration is due to the substantial chirp introduced by the ND filters. Using Femtosoft software in our analysis we obtain the spectral phase profile of the pulse (data not shown here). By using the standard procedure of Taylor series expansion of the obtained spectral phase profile [24] we found that the pulse yields a value for the GDD, $\beta_2 = 90$ fs^2 and using the value for τ_o found above (7 fs), the computed value for the broadened pulse duration (as estimated from Eq. (1)) is 38 fs. This value matches the experimentally observed pulse width of 42 fs very closely. The remaining small discrepancy (4 fs) between the computed and experimental values for the broadened pulse duration is most likely due to the fact that Eq. (1) above only includes the second order chirp (or GDD) term (generally the most dominant term). In reality some higher order terms may also be present which our analysis does not include.
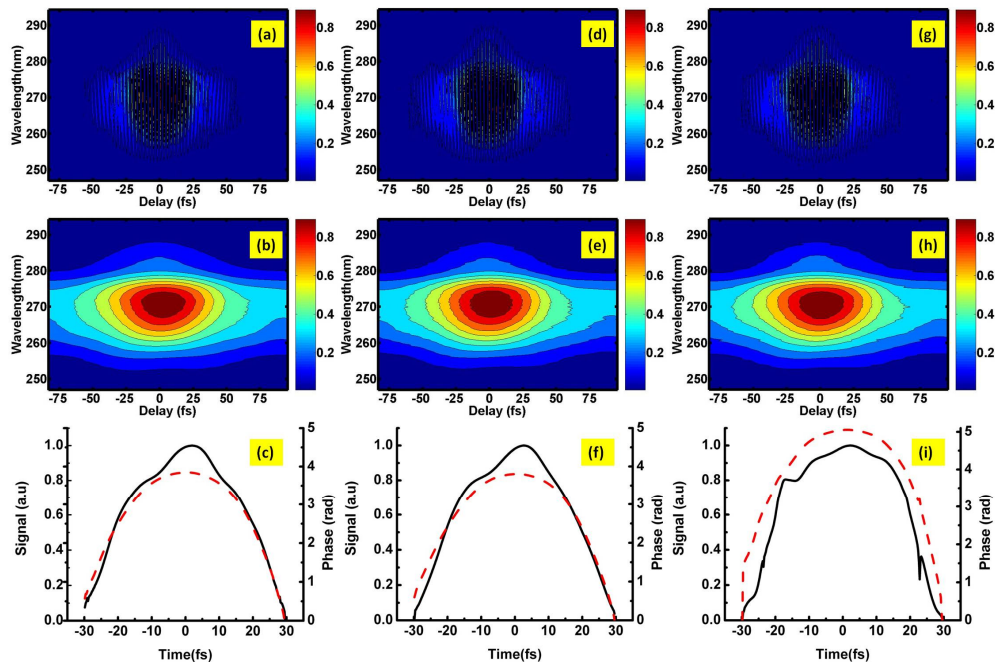

Fig. 4. iFROG trace, (b) FROG and (c) temporal pulse profile measured on ZnO nanorods grown by CBD growth method (with ND filter in path with optical density setting 0.04 + 0.04); (d) iFROG trace, (e) FROG and (f) temporal pulse profile measured on ZnO nanorods grown by CBD growth method (with ND filter in path with optical density setting 0.04 + 0.2); (g) iFROG trace, (h) FROG and (i) temporal pulse profile measured on ZnO nanorods grown by CBD growth method (with ND filter in path with optical density setting 0.04 + 0.4).

4. Conclusions

We have reported the use of ZnO nanorods grown by both CBD and VPT methods as efficient sources for third harmonic UV generation, with both growth methods showing very

comparable levels of THG. This result differs greatly from the case of the linear optical properties of ZnO nanorods grown by these two methods. The intensity dependence of the THG signal has been analysed and the third order nonlinear nature of signals in the region of 272 nm confirmed. The ZnO nanorod deposits give THG signals at least one order of magnitude greater than the STHG from the surface of a bare quartz sample indicating the intrinsic material suitability as an efficient generator of UV emission by up-conversion of red/near IR laser pulses. Furthermore, we have reported iFROG measurements on these samples, including extraction of the laser pulse parameters, and laser pulse broadening and chirping due to transmission through the ND filters used for certain measurements. These studies demonstrate that these nanorod deposits can be effectively used to characterize pulses generated by (originally) sub-10 fs laser pulses.

The efficiency of ZnO grown by these very different methods as sources for efficient third harmonic UV generation provides a broad range of potential growth methods which are compatible with various substrates, and offer different coverage and scalability capabilities. Readily achievable application areas include iFROG characterization of few cycle fs pulses and UV irradiation of single cells as part of biophysical studies.

Acknowledgments